Chemosphere 347 (2024) 140673

Contents lists available at ScienceDirect

Chemosphere

journal homepage: www.elsevier.com/locate/chemosphere

Assessing toxicity mechanism of silver nanoparticles by using brine shrimp (*Artemia salina*) as model

Sergimar Kennedy de Paiva Pinheiro [a], Ana Kamila Medeiros Lima [a], Thaiz Batista Azevedo Rangel Miguel [b], Antonio Gomes Souza Filho [c,**], Odair Pastor Ferreira [d], Montcharles da Silva Pontes [e], Renato Grillo [f], Emilio de Castro Miguel [a,*]

[a] *Biomaterials Laboratory (BIOMAT), Department of Metallurgical Engineering and Materials (DEMM) and Analytical Center, Federal University of Ceará - UFC, Campus do Pici, Fortaleza, Ce, Brazil*
[b] *Biotechnology Laboratory, Food Engineering Department, Federal University of Ceará - UFC, Campus do Pici, Fortaleza, Ce, Brazil*
[c] *Advanced Functional Materials Laboratory (LaMFA), Physics Department, Federal University of Ceará - UFC, Campus do Pici, Fortaleza, Ce, Brazil*
[d] *Advanced Functional Materials Laboratory (LaMFA), Chemistry Department, State University of Londrina - UEL, Londrina, PR, Brazil*
[e] *Optics and Photonics Group, SISFOTON Lab, Institute of Physics, Federal University of Mato Grosso do Sul (UFMS), Campo Grande, MS, Brazil*
[f] *School of Engineering, Department of Physics and Chemistry, São Paulo State University (UNESP), Ilha Solteira, SP 15385-000, Brazil*

HIGHLIGHTS

- AgNPs toxicity is also associated with the binding of ionic silver to the cuticle of *Artemia salina*.
- The deformation in the chitin structure is related to the ionic effect of AgNPs.
- The favorable coformation of Ag^+ with chitin was verified by computational analysis.
- Microscopy analysis showed AgNPs adhered to the cuticle and cellular damage.

GRAPHICAL ABSTRACT

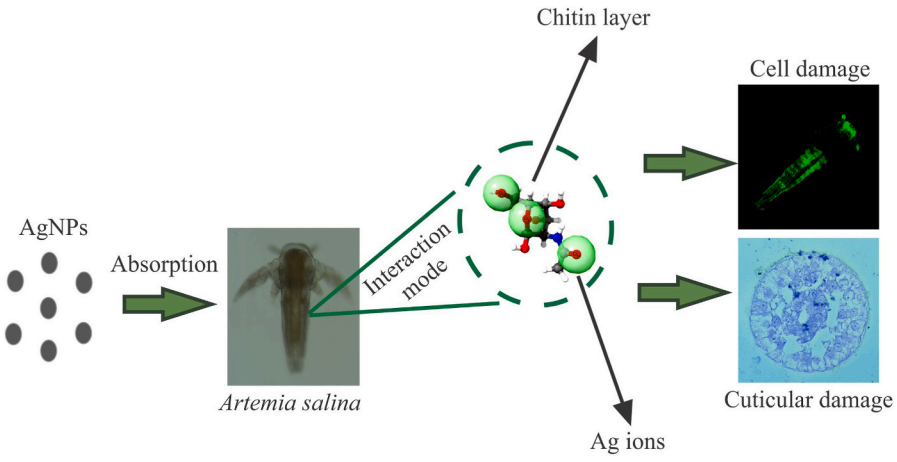

ARTICLE INFO

Handling Editor: Prof Willie Peijnenburg

Keywords:
Acute toxicity

ABSTRACT

The acute toxicity of silver nanoparticles (AgNPs) in *Artemia salina* is primarily attributed to the interaction between silver ions (Ag^+) and chitin, which constitutes the main structural component of the organism's cuticle. To investigate this interaction and gain a deeper understanding of its nature, geometric optimization calculations and symmetry-adapted perturbation theory (SAPT0) analysis were performed. These calculations aimed to

* Corresponding author. Universidade Federal do Ceará Campus do Pici Department of Metallurgical Engineering and Materials (DEMM) Biomaterials Laboratory (BIOMAT) CEP 60455-900 Fortaleza - Ceará - Brazil.
** Corresponding author.
E-mail addresses: agsf@fisica.ufc.br (A.G.S. Filho), emiliomiguel@ufc.br (E.C. Miguel).

https://doi.org/10.1016/j.chemosphere.2023.140673
Received 24 August 2023; Received in revised form 6 November 2023; Accepted 7 November 2023
Available online 9 November 2023

AgNPs
Artemia salina
Chitin
Computational chemistry
DFT

determine the most favorable conformation based on the binding energies of silver ions with chitin and to elucidate the underlying mechanisms of their interaction. The results indicate an ionic effect dependent on the ion state, with simulations revealing that Ag^{3+} ions have the potential to cause significant deformation of the chitin structure. Furthermore, this study evaluated the behavior of AgNPs using nauplii of *A. salina* instar I, assessing both mortality rates and cell damage. Toxicity of AgNPs was observed in *A. salina* at concentrations of 50 and 100 ppm within a timeframe of 24–48 h. The toxicity of AgNPs can be attributed to their interaction with the cuticle and subsequent modification of the chitin structure through the binding of ionic silver. Light microscopy (LM) analysis confirmed the presence of AgNPs in the cuticle, while confocal laser scanning microscopy (CLSM) revealed cellular damage. In addition, this research offers new perspectives on the toxicity mechanism of AgNPs by introducing a novel model that explores the interaction of silver ions with the cuticle of *A. salina*. These insights are derived from a combination of atomistic models and ecotoxicology assays.

Credit author statement

All authors contributed to the study conception and design. Developed research (Emilio de Castro Miguel). Write the manuscript (Sergimar kennedy de Paiva Pinheiro). Manuscript review and discussions (Thaiz Batista Azevedo Rangel Miguel, Renato Grillo and Antonio Gomes Souza Filho). Synthesis of AgNPs (Odair Pastor Ferreira). Performed the experiments (Ana Kamila Medeiros Lima). Computational analysis (Montcharles da Silva Pontes). All authors read and approved the final manuscript version.

1. Introduction

The development of nanotechnology was possible due to the development, innovation and commercialization of products with desirable characteristics in different areas (Meyer et al., 2009). In addition, developments in the field of nanotechnology have allowed the design and use of nanomaterials in a variety of products, such as cosmetics, electronic devices, pharmaceuticals and biomedical products, and water filters (Jin et al., 2010). Thus, nanoparticles (NPs) have been inserted in many technological applications (Adams et al., 2014) and it is a reality in many consumables that meet the societal needs. Currently, NPs have been used for various applications in different areas such as medicine (Alexiou, 2022; Yang et al., 2023), cosmetics (Mascarenhas-Melo et al., 2023), environmental remediation (Papolu and Bhogi, 2023), engineering (Ghadirian et al., 2023) and solar energy (Khairul Azri et al., 2023).

Increased demand for new products incorporating NPs raise concerns about human health and impact on ecosystems (Geisler-Lee et al., 2013; Tosco and Sethi, 2018), that inevitably reach the environment causing bioaccumulation (Ates et al., 2013). The NPs are contaminants that have unique physicochemical characteristics related to their surface area, energy quantum confinement (Christian et al., 2008), shape, surface coating and net charges (Mcgillicuddy et al., 2017) thus resulting in different fates and behaviors in the environment with various toxicity effects on biological organisms (Auffan et al., 2010; Lee et al., 2008). Among the main NPs described in the literature we can mention nanoparticles of graphene oxide (GO) (Rhazouani et al., 2023), selenium (Zeng et al., 2023), nickel (Ahamed et al., 2023), titanium (Machanlou et al., 2023), zinc (Ghouri et al., 2023) and silver (Tyagi et al., 2023). Silver nanoparticles (AgNPs) are among the most widely used NPs in the world due to their broad-spectrum antimicrobial activities (Mehennaoui et al., 2021).

In addition, AgNPs can be synthesized in different forms such as nanospheres, nanowires, nanorods, nanocubes and nanocoils (Bachenheimer et al., 2017). Currently, 920 tons of AgNPs are produced per year and it is said that more than 50% of nanomaterials contain AgNPs in their composition (Durán et al., 2019). With the increased production of AgNPs and their applications in different products, the disposal of this nanomaterial in the environment also increases, thereby making it necessary to investigate its environmental impacts and risks to human health (Eckhardt et al., 2013).

Plants, microorganisms, and animals exhibit vulnerability to the harmful impacts of NPs, prompting numerous studies across various species to evaluate the environmental risks associated with these nanomaterials (Yu et al., 2013). Several studies point to the acute toxicity of NPs in different aquatic organisms such as Algae (Zhang et al., 2023; Maia et al., 2024), *Daphnia magna* (Santos-Rasera et al., 2022), Zebra fish (Jafari et al., 2022; Krishnan et al., 2022) and *A. salina* (de Paiva Pinheiro et al., 2023; Monteiro et al., 2023). The primary toxicity of these NPs is associated with their physicochemical characteristics and their dissolution, which can generate reactive ions and cause damage to biological organisms (Kosa and Zaheer, 2022). In a toxicity study using AgNPs, an increase in ROS and degradation of enzymes in *A. salina* was observed within 48 h of exposure (An et al., 2019).

The toxicity of AgNPs is primarily attributed to the presence of Ag^{+} ions, with AgNPs serving as a direct source of these ions, further contributing to their toxic effects (Piccapietra et al., 2012; Xiu et al., 2012). For instance, research has demonstrated that the dissolved form of Ag^{+} ions exhibits greater toxicity compared to AgNPs themselves (Sendra et al., 2018). Within the marine environment, NPs can be ingested by animals, particularly zooplankton, posing a significant threat to organisms that rely on this food source for sustenance. (Ates et al., 2020; Lacave et al., 2017). NPs that accumulate in primary consumers, such as *Daphnia magna* and *A. salina*, can readily transfer through trophic levels, eventually reaching fish or crustaceans situated at higher positions in the food chain. Consequently, these NPs can offer a potential risk to humans through the consumption of contaminated aquatic organisms (Ates et al., 2020).

Artemia sp., commonly known as brine shrimp, is an invertebrate species belonging to the zooplankton. It can be found in various locations worldwide, inhabiting lakes and saline aquatic environments (Lavens and Sorgeloos, 1996). Due to its nutritional value, *Artemia* sp. is extensively utilized as a live food source to nourish the larvae of aquatic organisms in aquaculture practices (Sarkheil et al., 2018). Artemia's fast life cycle, high rate of reproduction, adaptability to laboratory conditions, and low maintenance costs make it an ideal model organism for toxicity testing purposes, including ecotoxicity assays. Its suitability as a test subject allows researchers to study the potential toxic effects of substances and assess their impact on aquatic ecosystems (Nunes et al., 2006; Manfra et al., 2014). The reliability and validity of ecotoxicological tests utilizing *A. salina* have been substantiated through numerous studies involving various stressors, such as NPs (Rekulapally et al., 2019), chemical compounds (Morgana et al., 2018), pesticides (Cruzeiro et al., 2017), and pharmaceutical substances (Nunes et al., 2006). These investigations have confirmed the effectiveness of *A. salina* as a model organism for assessing the potential ecological impact and toxicity of these stressors.

A. salina possesses a cuticle that covers its body, and during its developmental stages, the molting process initiates. This process encompasses an intricate series of biochemical and cellular events (Warner and Matheson, 1998). The molting process in *A. salina* takes place approximately 15–19 times throughout its life cycle, with the specific number of molts being influenced by the environmental conditions in which the organism resides (Anderson, 1967; Weisz, 1946). The cuticle is mainly composed of chitin (Zhang et al., 2021) and the interaction of

AgNPs with *A. salina* can modify the chitin structure thus causing toxicity as we will discuss.

The importance of employing combining classical toxicology assays with computational quantum-chemical calculations and molecular simulations, can offers a deeper understanding of the molecular-level interactions of nanomaterial and biological structures (Margiotta and Fonseca Guerra, 2021; Pontes et al., 2021), becomes evident their role and potential within the study of toxicity pathways (Santiago et al., 2020; Pontes et al., 2023). However, investigations related to mechanisms of interaction of chitin structure of *Artemia* cuticle and nanostructured Ag particles remain unclear. Also, quantum chemical methods play a crucial role in unraveling the intricate network of molecular associations, contributing to better understanding the potential toxicity mechanisms associated with the interaction of Ag ions with chitin.

In this sense, the present study aimed to investigate the *A. salina* nauplii instar I - acute ecotoxicity tests using AgNPs in different concentrations with an emphasis on mortality and cell damage. Additionally, the types of chemical interactions of Ag ions (Ag^0, Ag^+, Ag^{2+}, and Ag^{3+}) with chitin were investigated using a theoretical approach. In order to clarify the interaction between Ag ions and chitin structure, a computational study by applying quantum-chemical calculations were performed. Such findings may help understand the toxicity pathway and interaction mechanisms. We are proposing a model for understanding interaction mechanisms of AgNPs with the chitin structure.

2. Material and methods

2.1. Synthesis and characterization of AgNPs

The synthesis of silver nanoparticles (AgNPs) involved the citrate reduction method, with stabilization achieved using chitosan. The procedure consisted of adding 12 mL of a 15,000 mg/L silver nitrate solution and 1.5 mL of a 2% w/v chitosan propionate solution to 184 mL of deionized water. The mixture was vigorously stirred with a magnetic stirrer and heated to 100 °C. Then, a 2% w/v sodium citrate solution was added drop by drop (3.6 mL). After 5 min, 10 drops of a 1:1 v/v nitric acid solution were introduced. After an additional 1 min, the system was cooled in an ice bath until it reached room temperature. The size distribution and zeta potential of the colloidal silver nanoparticles were measured using a Nano ZS Zetasizer System (Malvern Instruments), with nine measurements taken for obtaining mean values. The absorption spectra of the colloidal nanoparticles were recorded using a Specord 250 spectrophotometer (Analytik Jena) with quartz cells of 1 cm optical path length. No dilution of the sample occurred prior to analysis. Surface analysis and determination of the silver nanoparticle diameter were performed using scanning electron microscopy (Quanta FEG 450 FEI) and transmission electron microscopy (JEOL 1011), respectively.

2.2. Test organism

A. salina cysts were procured from an aquaculture store located in Fortaleza, Ceará - Brazil. The dehydrated cysts were stored at a temperature of 4 °C and were utilized in all experimental procedures. The nauplii of instar I (24 and 48 h post-hatching) were obtained following the method outlined by Garaventa et al. (2010). In brief, 500 mg of cysts were incubated for 24 h at a temperature of 28 °C, under a light-dark cycle of 16 h of light and 8 h of darkness, while continuously aerating the cyst suspension in artificial seawater (ASW) with a salinity of 30%. The hatched nauplii were segregated from the unhatched cysts based on their positive phototaxis and were subsequently transferred into beakers containing ASW using a Pasteur pipette.

2.3. Acute toxicity test of AgNPs in A. salina

Acute exposure was conducted on nauplii instar I for 24 and 48 h according to (Johari et al., 2019) and Organization for Economic Cooperation and Development, OECD 202 testing guidelines (OECD, 2004). In summary, the study involved administering four different test concentrations (12.5, 25, 50, and 100 ppm) of AgNPs to nauplii at 24 and 48 h post-hatching. The negative control group was exposed to ASW, while the positive control group was exposed to potassium dichromate ($K_2Cr_2O_7$) at a concentration of 5 mM. The experiment was conducted in 24-well polystyrene microplates, with each well containing 2 mL of the respective solution. Each concentration was replicated three times, and each replication consisted of ten newly hatched nauplii. The room temperature was maintained at 24 °C, and a photoperiod of 12 h of darkness followed by 12 h of light was maintained. The number of dead larvae was subsequently counted under a stereomicroscope (Stemi 508) equipped with a ZEISS camera (Axiocam 208/202 mono). The validity of the test was determined based on a survival rate of $\geq$90% in the control group. (OECD, 2004).

2.4. Light microscopy (LM)

To analyze the accumulation of AgNPs, nauplii of instar I were collected at the 48-h mark of the experiment and washed with ASW. The nauplii were then carefully mounted on a glass slide, and images were captured using a Primo Star light microscope equipped with an axiocam color camera. Subsequent microscopy analyses, such as Confocal Laser Scanning Microscopy (CLSM), were conducted to observe any notable morphological variations resulting from acute AgNPs toxicity.

2.5. Confocal laser scanning microscopy (CLSM)

To evaluate cellular damage, acridine orange was utilized in nauplii of instar I exposed to different concentrations of AgNPs, along with negative control (ASW) and positive control ($K_2Cr_2O_7$). In brief, *A. salina* organisms were transferred to 24-well polystyrene microplates, with each well containing 3 mL of the respective solution. Then, 500 μL of acridine orange at a concentration of 5 μg/mL was added to each well and allowed to incubate for 20 min at room temperature. After incubation, the *A. salina* organisms were washed with phosphate buffer solution at pH 7.2. The stained samples were subsequently observed under a Confocal Laser Scanning Microscopy (CLSM) using 488 nm excitation and 532–580 nm emission wavelengths to detect any cellular damage.

2.6. Computational analysis

Chitin was computationally investigated using its respective monomer N-Acetyl-D-Glucosamine as a basic model by quantum chemistry (density functional theory) calculations. Geometry optimization and further modifications in the structure of the monomer chitin and respective complexes with Ag^0, Ag^+, Ag^{2+}, and Ag^{3+} ions were carried out using the Gaussian 09 program (Boyle et al., 2007), whereas the results are visualized by GaussView 5.0 software. Calculations, including geometry optimization for the molecule/molecular complex involved and electronic property calculations were carried out with the combination of BPW91/LANL2DZ basis sets in the gas phase, in a similar way as recommended to determine the interaction energies of organic molecules on silver metal systems (Legge et al., 2001). To account for the expected basis set superposition error (BSSE), which arises from the overlapping of infinite orbitals of interacting species, the counterpoise corrected method is employed when calculating the adsorption energies. This correction helps to eliminate the effects of BSSE and provides more accurate and reliable results in studying interactions between different species (Turi and Dannenberg, 1993).

The noncovalent interaction between two molecules can be directly computed using symmetry-adapted perturbation theory (SAPT0), that provide the interaction energy determined without computing the total energy of the monomers or dimers. The SAPT0 calculations were performed using PSI4 software (Turney et al., 2012) for evaluating the total

interaction energies of complexes (Chitin-Ag ions). Four main descriptors are used in the components of SAPT0 analysis and are normally given as: electrostatic (ΔEelstat), exchange (ΔEexch), dispersion (ΔEdisp), and induction (ΔEind). The equation for ΔEint in SAPT0 analysis is given according to equation [e.q. 01]:

$$\Delta_{Eint} = \Delta_{Eexch} + \Delta_{Eelast} + \Delta_{Eind} + \Delta_{Edis} \quad [Eq.1]$$

In equation 01, the complexes are stabilized by the electrostatic, dispersion, and induction components, as these processes release energy (exothermic). The electrostatic component arises from the attractive coulombic interactions between two opposite charges. The dispersion component is a result of instant charge fluctuations, leading to attractive interactions. The induction component arises from dipole-induced dipole interactions, contributing to the overall stabilization of the complexes.

On the other hand, the exchange component in ESAPT0 acts as a repulsive force, destabilizing the complexes. This repulsion arises from Pauli repulsion, which occurs due to the overlapping of orbitals. The exchange component accounts for the exclusion principle and prevents excessive electron density overlap, ultimately leading to destabilization of the complexes (Sajid et al., 2018).

Therefore, in order to find interatomic clashes (unfavorable interactions) from chitin molecule to AgNP surface, we also apply the empiric docking method, based on a hybrid algorithm of template-based modeling and ab initio free docking (Yan et al., 2016). Geometry optimized chitin molecule was used as ligand, and an AgNP was modeled with 1865 atoms and a particle diameter size of 1.0 nm, using Nano-Crystal tool (Chatzigoulas et al., 2018) and modeled nanoparticle is presented in Fig. S1 (Supporting information).

2.7. Statistical analysis

The data obtained from the experiments were recorded daily and presented as the mean values along with their corresponding standard deviations for statistical analyses. The normality of the data and the significance of the differences were evaluated using the R environment, specifically utilizing the psych package. To assess the normality of the data, the Shapiro-Wilk test was employed, as it is appropriate for datasets with a sample size (n) of less than 30. This test was performed using the shapiro.test function in R. Additionally, the *t*-test was utilized to determine the significance of differences between the means of each treatment group (12.5, 25, 50, 100 ppm) relative to the control treatment (ASW). The *t*-test function in R was employed for this analysis.

3. Results and discussion

3.1. Physico-chemical characterization of the AgNPs

In this study, the AgNPs utilized were stabilized with chitosan, resulting in a positive surface charge of +40.8 mV, as determined by zeta potential analysis. This positive charge helps prevent the agglomeration of nanoparticles, as previously described (Edison and Sethuraman, 2012; Pontes et al., 2021). By employing stabilizers such as chitosan, the colloidal stability of the nanoparticles was enhanced, ensuring that the suspension remains stable for an extended period(Cedervall et al., 2007). Nanoparticles aggregation can alter the toxicity of the nanoparticle (Ates et al., 2020; Bai et al., 2010). The size distribution of the AgNPs was determined based on data obtained from dynamic light scattering (DLS), along with the UV/Vis absorption spectrum. These measurements indicated an average diameter of 15 nm for the AgNPs. The analysis carried out by Transmission Electron Microscopy (TEM) confirmed the presence of irregular shapes, including spherical and ovoid surfaces as evidenced by an article previously published by our group (De Paiva Pinheiro et al., 2020).

Similar results related to the characterization of AgNPs were observed by several authors (Muthukrishnan et al., 2017; Wang et al., 2019). In another study, the AgNPs size ranged from 30 to 50 nm with a spherical surface with a wrinkled surface (Muthukrishnan et al., 2017). The size of the NPs, is directly associated with surface/volume and smaller NPs are generally more toxic to biological systems as observed by (Ates et al., 2020). Indeed, AgNPs can exhibit diverse physicochemical characteristics, including variations in size, shape, surface coatings, and charges. These factors significantly influence the behavior, fate, and potential toxic effects of AgNPs on living organisms. Differences in size can affect the stability and reactivity of AgNPs, while variations in shape can impact their surface area and interactions with biological systems. Surface coatings, such as chitosan or other stabilizers, can alter the surface charge and interactions with cellular components. The overall physicochemical characteristics of AgNPs play a crucial role in determining their behavior in biological systems, their potential for uptake by organisms, and the subsequent toxic effects they may exert (Mcgillicuddy et al., 2017). The full characterization of the AgNPs used in this study is reported by De Paiva Pinheiro et al. (2020)

3.2. Acute toxicity test

During the 24-h exposure of *A. salina* nauplii instar I to AgNPs, no mortality was observed at the concentrations of 12.5 and 25 ppm, which showed similar results to the negative control (ASW) (Fig. 1). However, at higher concentrations of AgNPs (50 and 100 ppm), a significant increase in mortality rate was observed for nauplii instar I at both 24 and 48 h of exposure (Fig. 1). The statistical analysis, indicated by a P-value of less than 0.05, confirmed the significant difference between these higher AgNPs concentrations and the negative control, as presented in Table 1.

The similarity in results observed between the AgNPs exposure and the study evaluating the interaction of $K_2Cr_2O_7$ in nauplii instar I is noteworthy (Ocaranza-Joya et al., 2019). The high mortality observed in both cases is unexpected because at this stage, *A. salina* is typically considered less sensitive to contaminants due to the incomplete development of their mouth and gut (Sorgeloos et al., 1978). However, these findings suggest that the tested substances, both AgNPs and $K_2Cr_2O_7$, may have significant toxic effects on *A. salina* nauplii instar I, possibly through alternative pathways or mechanisms of toxicity that are not solely dependent on oral ingestion. The toxicity of AgNPs may be related to the binding of silver ions to chitin during the molting process in *A. salina* that occurs between 18 and 24 h after hatching (Anderson, 1967; Freeman, 1986; Warner and Matheson, 1998). AgNPs can bind to the chemical structure of the cuticle which is mainly composed of chitin (Chang, 1995). In addition, structural changes in chitin caused by silver ions binding subsequently lead to the accumulation of AgNPs in *A. salina* cells thus causing toxicity.

3.3. AgNPs accumulation

All microscopy analyzes were performed for *A. salina* exposure of 48 h to AgNPs. The accumulation of AgNPs was examined using light microscopy (LM). When nauplii instar I were observed in ASW, they exhibited a translucent body without the presence of particles (Fig. 2A). Additionally, the cells appeared turgid, as depicted (Fig. 2B). At the concentration of 12.5 ppm, no accumulation of AgNPs was observed in the gut of *Artemia* nauplii (Fig. 2C). Furthermore, there was no evidence of cell damage in the observed cells (Fig. 2D). Similar results were observed at the concentration of 25 ppm, where no AgNPs accumulation was detected in the gut of *Artemia* nauplii (Fig. 2E) and no cell damage was observed (Fig. 2F). At the higher concentration of 50 ppm of AgNPs, no accumulation was observed in the gut of *Artemia* nauplii (Fig. 2G). However, the accumulation of AgNPs was observed in the cuticle of the nauplii at the same concentration (Fig. 2H). Similar results were also observed at the concentration of 100 ppm of AgNPs, where no accumulation of AgNPs was detected in the gut of the nauplii (Fig. 2I and J).

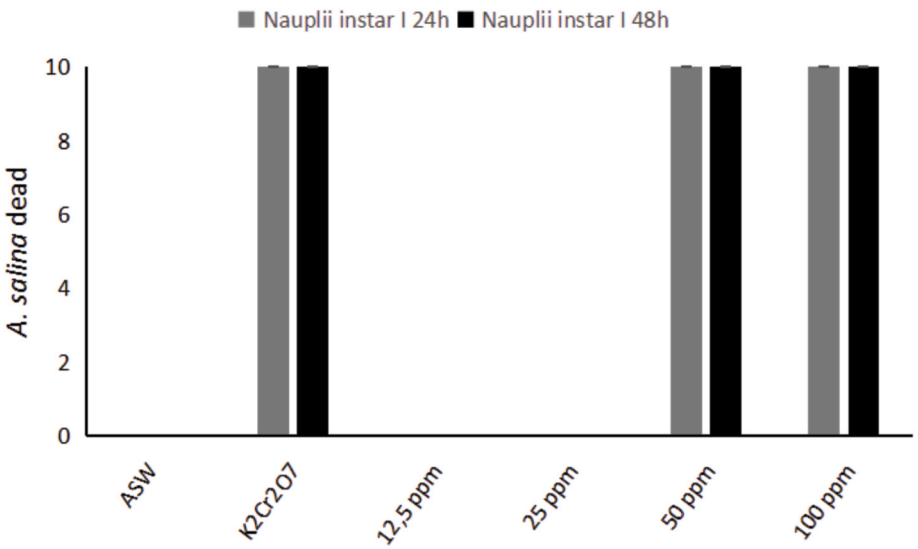

Fig. 1. Acute toxicity of AgNPs in *Artemia salina* nauplii instar I and instar II within 24 h and 48 h of exposure. Mortality was observed at 24 and 48 h at AgNPs concentrations of 50 and 100 ppm. The experiment was performed in triplicate. Mean ± standard deviation (σ) for all standards. Significant difference between negative control - ASW and *A. salina* exposed to AgNPs are symbolized by an asterisk * (*t*-test, $P < 0.05$).

Table 1
Acute toxicity of AgNPs in *A. salina* nauplii instar I and percentage of individuals dead within 24 and 48 h. At this stage of development, toxicity of AgNPs was observed at 50 ppm and 100 ppm concentrations. Mean ± standard deviation (σ) obtained from the triplicate in each treatment. The significant difference between ASW and *A. salina* exposed to AgNPs is represented by asterisks * (*t*-test, $P < 0.05$).

A. salina - nauplii instar I						
24 h of exposure				48 h of exposure		
Treatments	Mean ± SD of living individuals	*P-value*	% Mortality	Mean ± SD of living individuals	*P-value*	% Mortality
ASW	10.0 ± 0.0	-	0%	10.0 ± 0.0	-	0%
$K_2Cr_2O_7$	0.0 ± 0.0*	***P ≤ 0.01****	100%	0.0 ± 0.0*	***P ≤ 0.01****	100%
12.5 ppm	10.0 ± 0.0	*P = NA*	0%	10.0 ± 0.0	*P = NA*	0%
25 ppm	10.0 ± 0.0	*P = NA*	0%	10.0 ± 0.0	*P = NA*	0%
50 ppm	0.0 ± 0.0	***P = 0.01****	100%	0.0 ± 0.0	***P = 0.01****	100%
100 ppm	0.0 ± 0.0	***P = 0.01****	100%	0.0 ± 0.0	***P = 0.01****	100%

This can be attributed to the incomplete development of the mouth and digestive tract at this life stage, which may limit the uptake and accumulation of AgNPs in the gut (Sorgeloos et al., 1978). However, the presence of AgNPs in the cuticle suggests that uptake and accumulation through other pathways, such as direct contact with the external surface, may still occur. As expected, a positive control group ($K_2Cr_2O_7$) presented morphological damage to the animal's body (Fig. 2K and L).

3.4. Cell damage analysis

To evaluate the potential cellular damage induced by AgNPs in the *A. salina* model, acridine orange was employed in nauplii instar I that had been exposed to AgNPs for 48 h. The use of acridine orange in confocal microscopy enables the identification of cells undergoing apoptosis. Acridine orange binds to the DNA of cells undergoing apoptosis, resulting in the emission of green fluorescence in the wavelength range of 488–535 nm. By utilizing acridine orange in this manner, it becomes possible to visualize and assess the presence of apoptotic cells in the *A. salina* nauplii instar I population exposed to AgNPs (Damas-Souza et al., 2019; Muthukrishnan et al., 2017). In the control group (ASW), a low green fluorescent emission was observed, indicating the preservation of cells (Fig. 3A). In contrast, the positive control group exposed to $K_2Cr_2O_7$ exhibited strong green fluorescence emission, indicating significant cell damage (Fig. 3B). Nauplii instar I exposed to the low concentration of AgNPs (12.5 ppm) showed a result similar to the ASW control group, with minimal green fluorescence emission (Fig. 3C). At the concentration of 25 ppm, numerous fluorescent spots were observed on the body of the *Artemia* nauplii, indicating potential cellular uptake of AgNPs (Fig. 3D). Upon increasing the concentration of AgNPs to 50 ppm, a strong green fluorescence emission was observed, indicating significant cell damage (Fig. 3E). Similar results were observed at the highest concentration tested, 100 ppm, indicating cellular damage in nauplii instar I caused by AgNPs (Fig. 3F). At this maximum concentration, a high fluorescence emission was observed, indicating marked damage to the cells caused by the AgNPs. The greatest damage was observed in the cells of the gut of *A. salina* due to the accumulation of AgNPs (Alexiou, 2022; Yang et al., 2023). The absorption and interaction of NPs alter cellular dynamics due to the inactivation of enzymes, degradation of lipids and binding of Ag^+ to DNA, promoting cell death. Similar result was observed by Arulvasu et al. (2014) using AgNPs in *A. salina* at 12 nM concentration.

3.5. Interaction model of silver ions with the chitin

3.5.1. Geometry optimization

Here, the stabilities of chitin are compared upon complexation with Ag ions (Ag^0, Ag^+, Ag^{2+}, and Ag^{3+}). Firstly, all the possible adsorption geometries are optimized to get the most suitable confirmation based on the electronic energies. The most stable optimized geometric conformations (given in Fig. 4A and B) are selected for detailed analysis. Fig. 4 illustrates that the Ag ions (Ag^0, Ag^+, Ag^{2+}, and Ag^{3+}) are able to interact with the chitin molecule. Our results reveal that Ag ions can

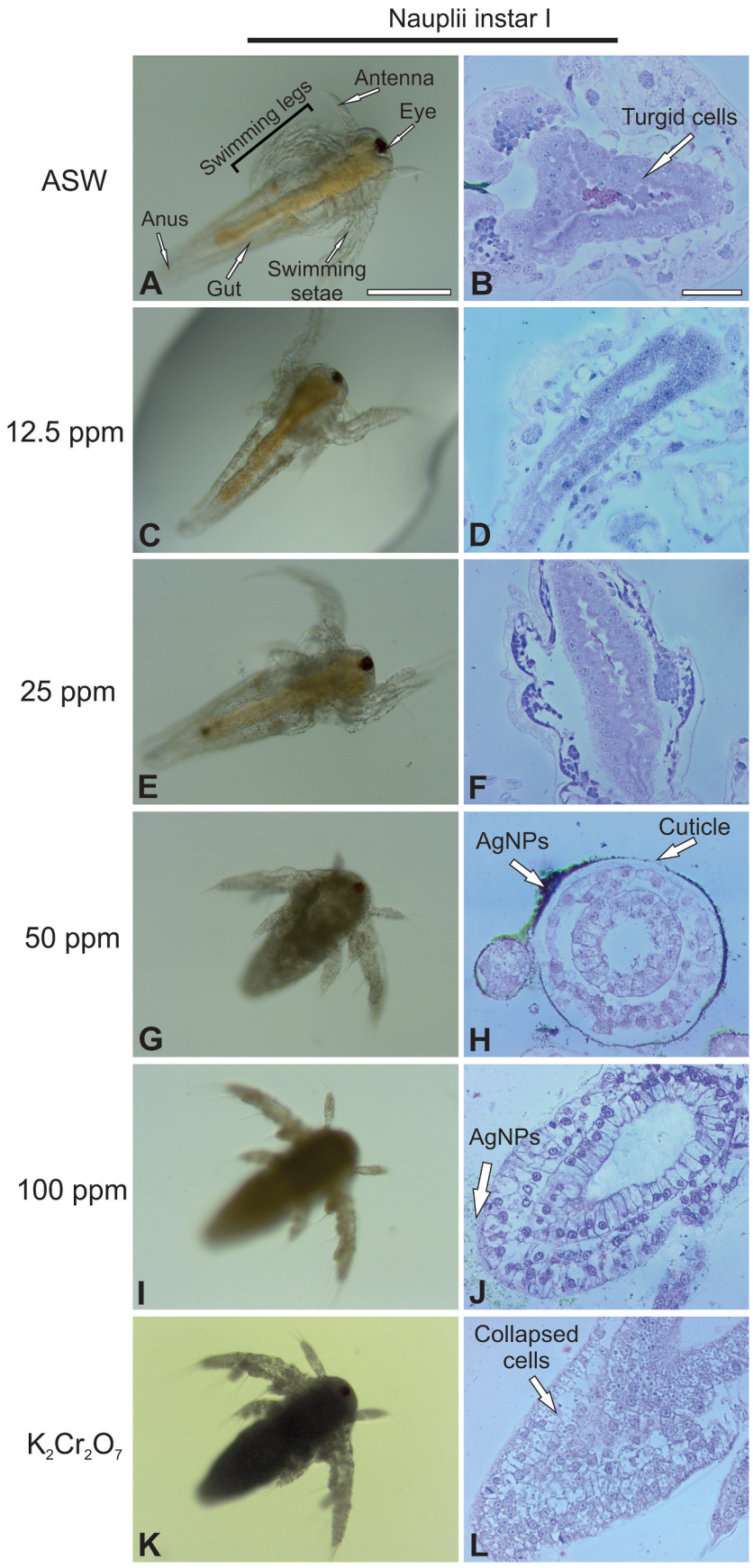

(caption on next page)

Fig. 2. Optical microscopy and historresin in *A. salina* nauplii instar I within 48 h of exposure to AgNPs. A – Negative control (ASW); B – *A. salina* with intact and turgid cells; C – No accumulation of AgNPs at a concentration of 12.5 ppm; D – Cells without damage; E – No accumulation of AgNPs was observed at 25 ppm; F – *A. salina* with preserved cells, similar to the control group (ASW); G – At the concentration of 50 ppm, *A. salina* did not develop, presenting a high mortality rate; H – AgNPs adhered to the cuticle of nauplii; I – *A. salina* submitted to a concentration of 100 ppm of AgNPs. In this concentration, a high percentage of mortality was observed; J – Cuticle of *A. salina* with accumulation of AgNPs; K – Positive control ($K_2Cr_2O_7$); L – *A. salina* with collapsed cells. Bars: A, C, E, G, I, and K - 200 μm; B, D, F, H, J, and L - 20 μm.

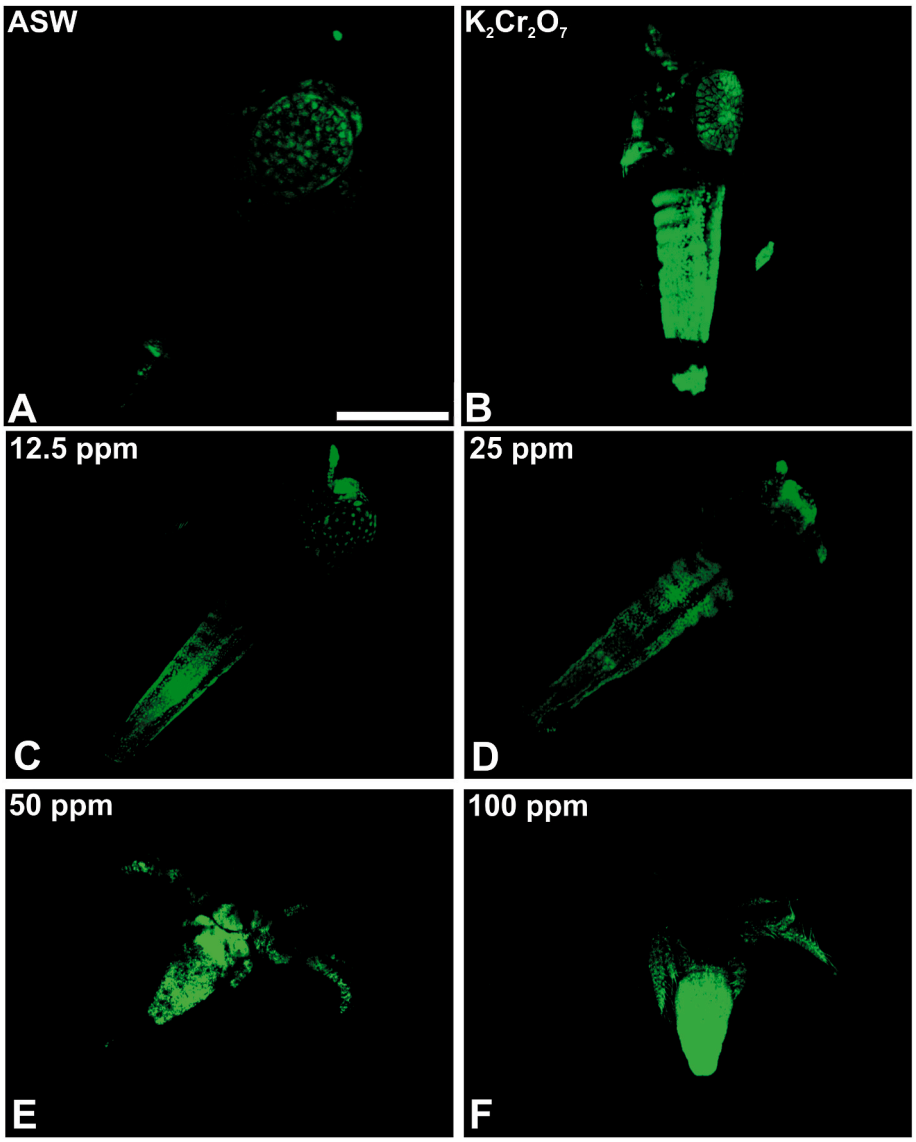

Fig. 3. Acridine orange showing cell damage in *A. salina* nauplii instar I within 48 h of exposure. A – Negative control (ASW); B - Positive control ($K_2Cr_2O_7$); C, D - *A. salina* subjected to a concentration of 12.5 ppm and 25 ppm of AgNPs presented low emission of the fluorophyll; E, F – At the concentration of 50 ppm and 100 ppm, high emission of the fluorophile was observed, indicating cell damage. Bar: 200 μm.

bind the C–*O*–C from hexose, –$NHCOCH_3$ from the N-acetyl group, and –CH_2OH from the hydroxymethyl group, respectively. However, the interaction domain is dependent on the redox state of the Ag ion, and this changing mode of interaction might be responsible for the toxicity behavior AgNPs to *A. salina* cuticle barrier. According to Fig. 4 (J-L) results, Ag^{3+} ion adsorption onto chitin totally deforms the structure of the chitin molecule; this probably reveals the peculiar role of Ag^{3+} ions from AgNP surface and chitin interface in case of AgNPs agglomeration around the cuticle layer in *A. salina* or nanoparticle ionic release from its dissolution in the extracellular space.

The interaction parameters including, interacting atoms (A_{int}), the functional group of these atoms, adsorption distances (D_{int}), and adsorption energies (E_{int}) are given in Table 2A. The adsorption energy describes the physisorption or chemisorption nature of interactions between Ag ions and chitin. The interaction energy (E_{int}) trend of studied complexes is Ag^{3+}-chitin (i) −39.62 eV (−913.72 kcal/mol^{-1}) > Ag^{3+}-chitin (ii) −39.25 eV (−905.13 kcal/mol^{-1}) > Ag^{3+}-chitin (iii) −39.08 eV (−901.25 kcal/mol^{-1}) > Ag^{2+}-chitin (i) −14.14 eV (−326.10 kcal/mol^{-1}) > Ag^{2+}-chitin (ii) and Ag^{2+}-chitin (iii) −13.88 eV (−320.04 kcal/mol^{-1}) > Ag^{+}-chitin (ii) −2.943 eV (−67.87 kcal/mol^{-1}) > Ag^{+}-chitin (iii) −2.912 eV (−67.16 kcal/mol^{-1}) > Ag^{+}-chitin (i) −2.752 eV (−63.46 kcal/mol^{-1}) > Ag^{0}-chitin (i) −0.253 eV (−5.84 kcal/mol^{-1}) > Ag^{0}-chitin (ii) and Ag^{0}-chitin (iii) −0.243 eV (−5.61 kcal/mol^{-1}). The lowest intermolecular distances (D_{int}) are observed for Ag^{0}–O_{12} and Ag

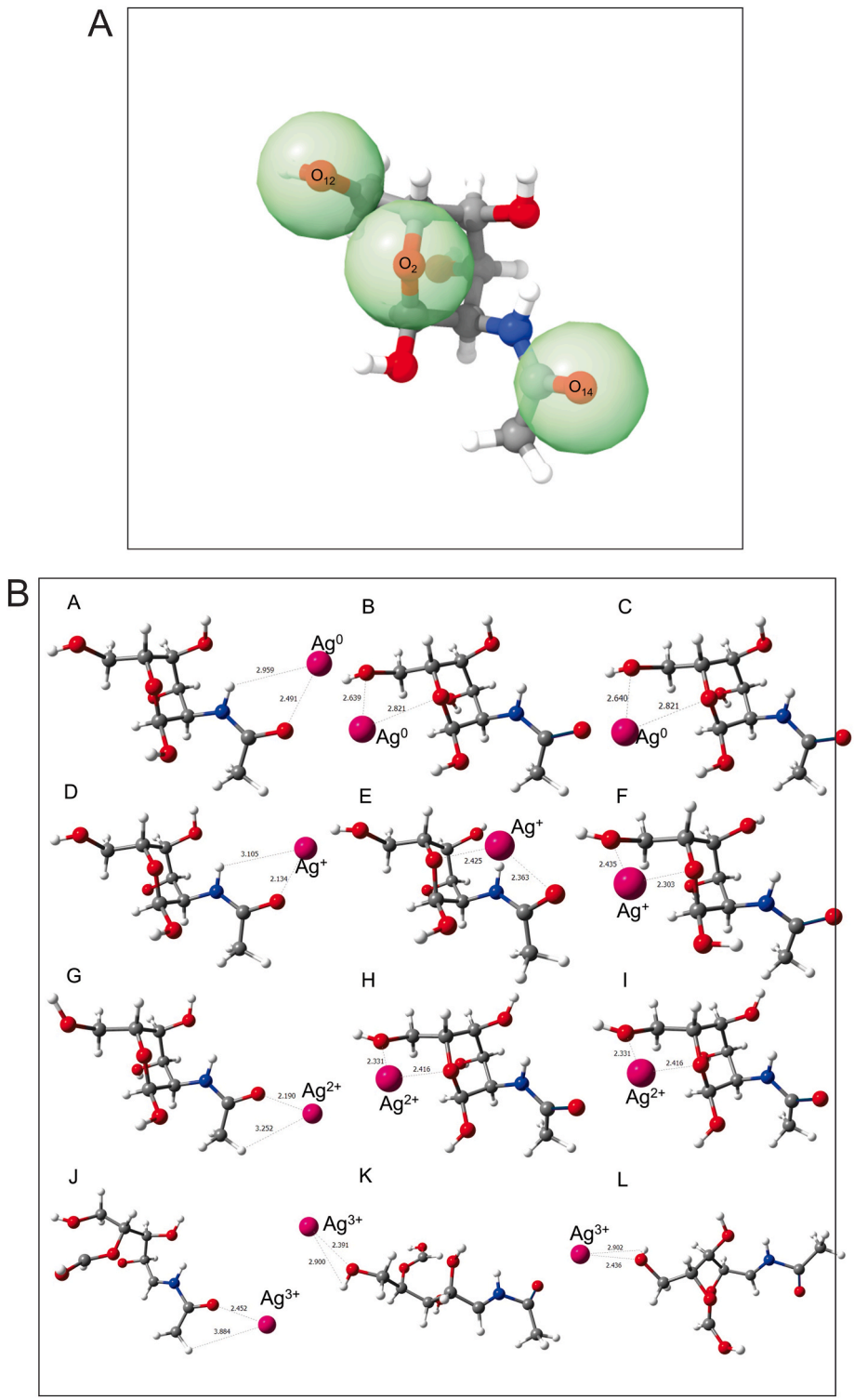

Fig. 4. - A - Optimized structure for the monomer of chitin at BPW91/LANL2DZ basis level of theory in the gas phase. Inset in green represents the most favorable Ag ions bind region of chitin molecule; B - Optimized structures for the monomer of chitin complexed with Ag^0, Ag^+, Ag^{2+}, and Ag^{3+} at BPW91/LANL2DZ basis level of theory in the gas phase.

$^+$ -O_{12} with a distance of 1965 Å, and the highest intermolecular distances are presented by Ag^{2+-}chitin (ii), Ag^{2+-}chitin (iii) and Ag^{3+-}chitin (iii) with O_{12}, respectively.

Interaction energy results reveal that the mechanisms involved adsorption of Ag ions with chitin are considered to be physisorption (Sarfaraz et al., 2022). The interaction energy in physisorption must be less than <~1 eV and it has been extensively reported in the literature (Asif et al., 2021). Small interaction energy (eV) values observed in our results strongly suggest that all studied Ag ions are physisorbed onto chitin molecules in the cuticular layer of *A. salina*. Additionally, these higher interaction energies observed for Ag^{3+} ions corroborate our proposed hypothesis of potential disruption of the cuticle layer through structural deformation of the chitin molecule. The interaction of Ag^{3+} ions with chitin leads to significant structural deformation of the chitin

Table 2
- A - The results of the most stable optimized complexes of chitin bonded with Ag^0, Ag^+, Ag^{2+}, and Ag^{3+} ions at BPW91/LANL2DZ basis level of theory in the gas phase; B - Tabular data of HOMO LUMO energies for the most stable optimized complexes of chitin bonded with Ag^0, Ag^+, Ag^{2+}, and Ag^{3+} ions at BPW91/LANL2DZ basis level of theory in the gas phase.

A

Complex	A_{int}	Functional group	D_{int} (Å)	E_{int} (kcal/mol^{-1})
Ag^0-chitin (i)	Ag^0–O_{14}	N-acetyl	2.237	−5.84
Ag^0-chitin (ii)	Ag^0–O_2	Hexose	2.248	−5.61
Ag^0-chitin (iii)	Ag^0–O_{12}	Alcohol	1.965	−5.61
Ag^+-chitin (i)	Ag^+-O_{14}	N-acetyl	2.237	−63.46
Ag^+-chitin (ii)	Ag^+-O_2	Hexose	2.248	−67.87
Ag^+-chitin (iii)	Ag^+-O_{12}	Alcohol	1.965	−67.16
Ag^{2+}-chitin (i)	Ag^{2+}-O_{14}	N-acetyl	2.491	−326.10
Ag^{2+}-chitin (ii)	Ag^{2+}-O_{12}	Alcohol	2.915	−320.04
Ag^{2+}-chitin (iii)	Ag^{2+}-O_{12}	Alcohol	2.640	−320.04
Ag^{3+}-chitin (i)	Ag^{3+}-O_{14}	N-acetyl	2.134	−913.72
Ag^{3+}-chitin (ii)	Ag^{3+}-O_{12}	Alcohol	2.639	−905.13
Ag^{3+}-chitin (iii)	Ag^{3+}-O_{12}	Alcohol	2.640	−901.25

B

Complex	HOMO (eV)	LUMO (eV)	Egap (eV)
Ag^0-chitin (i)	−3.01797	−0.78313	−2.23484
Ag^0-chitin (ii)	−3.78178	−0.84762	−2.93416
Ag^0-chitin (iii)	−3.78151	−0.84789	−2.93362
Ag^+-chitin (i)	−8.55405	−7.4882	−1.06585
Ag^+-chitin (ii)	−9.10426	−6.35595	−2.74831
Ag^+-chitin (iii)	−8.27677	−6.97772	−1.29905
Ag^{2+}-chitin (i)	−13.0733	−9.97446	−3.09879
Ag^{2+}-chitin (ii)	−13.6139	−10.1198	−3.49416
Ag^{2+}-chitin (ii)	−13.6139	−10.1198	−3.49416
Ag^{3+}-chitin (i)	−16.7693	−14.4934	−2.27593
Ag^{3+}-chitin (ii)	−16.2501	−13.3802	−2.86994
Ag^{3+}-chitin (iii)	−16.2861	−13.6972	−2.58885

molecule, indicating a specific and notable mode of interaction that might be linked to repulsive forces and the potential disruption of the cuticle layer, a key point inferred from our study. We observed that the induction and dispersion forces also contribute to the stability of the Ag ions-chitin complexes.

The energy gap between the highest occupied molecular orbital (HOMO) and lowest unoccupied molecular orbital (LUMO) is fundamental in understanding the chemical reactivity and stability of Ag ion-chiton complex. The energy gap difference between the HOMO and LUMO for Ag ions-chitin monomer complexes of BPW91/LANL2DZ basis sets level is presented in Table 2B. The energy of the smaller band space gap of Ag^+-chitin (i) and Ag^+-chitin (iii) suggest an increase in the reactive nature and stability, which also corroborates with our findings of stable interaction of Ag^+ ions with O_{14} and O_{12} from N-acetyl and alcohol functional groups in chitin molecule, respectively. On the other hand, the energy of higher band space of Ag^{2+}-chitin (ii) and Ag^{2+}-chitin (iii) reveals a decrease in the reactive nature and stability, suggesting that these bonds may evidence unfavorable interactions. Additionally, the electronic transitions HOMO and LUMO involving chitin and Ag ions interactions are presented in Figure S2 (Supporting information) for illustrating the specific sites of interaction within the chitin structure for each Ag ion, for chitin complexes with Ag^0, Ag^+, Ag^{2+} and Ag^{3+} ions, respectively. Also, we emphasized the importance of these transitions, specifically in relation to the adsorption values, by explaining how these energy gaps represent the reactive nature and stability of the interactions between Ag ions and distinct functional groups within the chitin molecule. This relationship between the transitions and adsorption values is pivotal, as a smaller energy gap generally signifies heightened reactivity. Therefore, these transitions directly impact the adsorption behavior by providing a molecular-level insight into the affinity and stability of Ag ions with specific molecular sites within the chitin structure, influencing their adsorption capacities and behaviors within the chitin matrix.

3.5.2. SAPT0 analysis

Symmetry-adapted perturbation theory (SAPT0) analysis is utilized to quantitatively assess and comprehend the interactions between chitin and Ag ions. SAPT0 analysis involves four key components that contribute to the interaction energy. This analytical approach serves as a valuable tool in gaining insights into the physical nature of non-covalent bonding, providing a detailed understanding of the interactions between chitin and Ag ions (Khan et al., 2020). The attraction between Ag ions and chitin that stabilizes the complexes is attributed to the exothermic nature of the electrostatic, induction, and dispersion components. However, the exchange component is endothermic, reflecting the repulsive forces and the unstable nature of the complexes (Sarfaraz et al., 2022). Thus, our results in the contribution of SAPT0 components for Ag^0-chitin complex toward total ΔE_{SAPT0} (Fig. 5A), illustrate that the electrostatic component dominates in the complexes among the three intermolecular interactions of Ag^0 with chitin (Ag^0–O_{14}, Ag^0–O_2, Ag^0–O_{12}) which values are −28.42, −32.97, and −32.96 kcal/mol^{-1} respectively. The ΔE_{Elst} is crucial in stabilizing complexes, while ΔE_{Exch} component is responsible for destabilizing the complexes (Asif et al., 2021; Sarfaraz et al., 2022). The induction component also contributes significantly to the stability of Ag^0-chitin complexes, as electrostatic interaction does.

The overall order of contribution of SAPT0 components for Ag^+-chitin complex toward total ΔE_{SAPT0} presents the following trend $\Delta E_{Elst} > \Delta E_{Ind} > \Delta E_{Dist}$. Fig. 5A (B). These SAPT0 component values suggest that the electrostatic component plays a major role as stabilizing factor for Ag^+-chitin complexes, which presents attractive forces between interacting components i.e., Ag^+ and chitin. The trend of total ΔE_{SAPT0} for Ag^+ -chitin complexes shows an acceptable agreement with the interaction energy results. The contribution of the induction component also contributes significantly to the stability of Ag^+-chitin complexes. The exchange part (ΔE_{Exch}) of SAPT0 analysis is revealing the existence of repulsive force between the filled orbitals of two interacting components, with a major contribution for Ag^0 and Ag^+ ions. These repulsive forces could act on AgNP surface, due to the metallic silver nature of the nanostructure and the release of Ag ions (Forini et al., 2022; Mezacasa et al., 2020). On the other hand, the induction component dominates in the complexes among the three intermolecular interactions of Ag^{2+} and Ag^{3+} ions with chitin, followed by the electrostatic component Fig. 5A (C, D), whereas the exchange component is a less dominant contribution, as compared with A^0 and Ag^+ ions bonded with chitin, towards the total SAPT0, respectively. Finally, the general trend of total SAPT0 interaction energies is as follow: Ag^{3+-}chitin (ii) > Ag^{3+-}chitin (iii) > Ag^{3+-}chitin (i) > Ag^{2+-}chitin (iii) > Ag^{2+-}chitin (ii) > Ag^{2+-}chitin (ii) > Ag^{+-}chitin (ii) > Ag^{+-}chitin (iii) > Ag^{+-}chitin (i) > Ag^{0-}chitin (i) > Ag^{0-}chitin (ii) > Ag^{0-}chitin (iii).

3.5.3. Ab initio free docking of chitin onto the AgNP surface

Molecular docking is a powerful computational tool wherein the interaction between the ligand and its binding site, or ligand–nanoparticle complex can be studied at the atomistic level (Meng et al., 2012; Narayan et al., 2022; Pontes et al., 2021; Yadav et al., 2018). The adsorption of chitin molecules on the AgNP surfaces was predicted by docking simulation Fig. 5B (A, B). We used AgNPs without the chitosan coating in the simulation because the chitosan polymer has a chemical structure similar to chitin, not interfering with the binding sites. The chitin molecules could interact with AgNP surface. Based on the docking results, the most stable pose conformation of the chitin molecule was considered to study its interaction and orientation on the AgNP surfaces. During the simulation, it was observed that the chitin monomer did not present any clashes, but in polymeric form, non-polar hydrogen from OH in –CH_2–OH presented a strong clash with Ag^{2+} ions on the AgNP surface, and Ag^+ clashed with the oxygen from C–*O*–C Fig. 5B (C, D). Furthermore, our docking results also corroborate with DFT calculations Fig. 5B (E), and showed interactions with Ag^0, Ag^+, Ag^{2+} and Ag^{3+} ions, respectively, for the pose with the highest docking

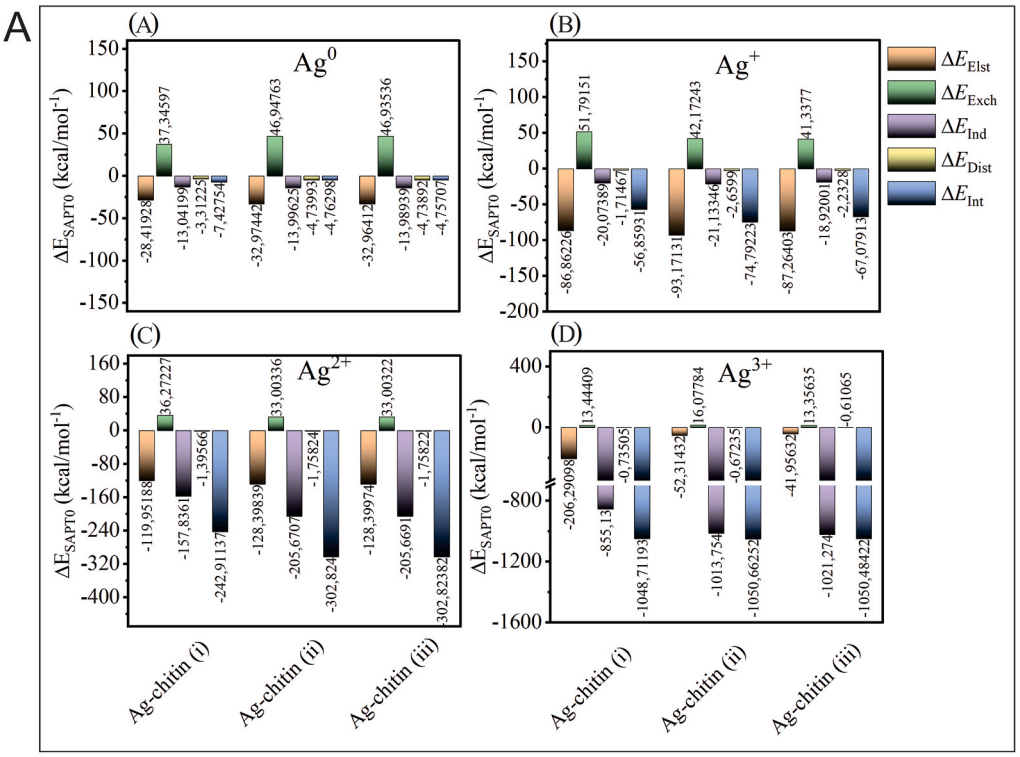

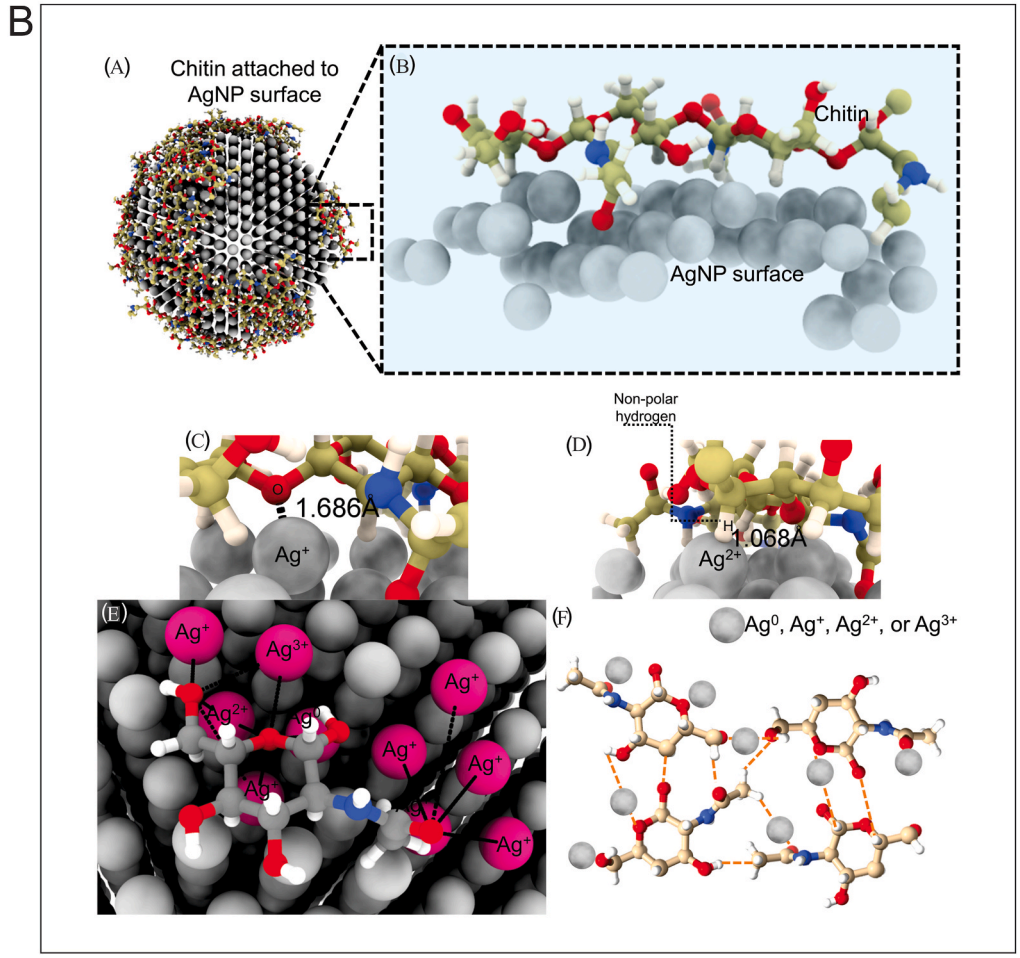

(caption on next page)

Fig. 5. - A - Graphical decomposition representation of the contribution SAPT0 energies components in the most stable optimized complexes of chitin bonded with Ag^0, Ag^+, Ag^{2+}, and Ag^{3+} ions; B - (A - Trimeric chitin oligomer attached to a silver nanoparticle; B - detailed view of the AgNP surface; C, D - Ag ions at AgNP surface clashed with the oxygen and hydrogen of the chitin molecule; E – Pose with the highest score in docking analysis, corroborate with ionic type insight; F - proposed regions of AgNP interaction with the chitin network).

score. As expected, simulations showed the potential toxicity pathway of AgNP onto the cuticle barrier through the chitin interface. In general, our findings suggest that AgNPs can modify the structure and function of chitin molecules Fig. 5B (F).

4. Conclusions

The present study investigates the interaction between AgNPs and *A. salina* through a combination of toxicology assays and atomistic modeling. The results indicate that AgNPs at concentrations of 50 and 100 ppm exhibited toxicity towards nauplii instar I after 24 h of exposure. The toxicity mechanisms of AgNPs in *A. salina* appear to be associated with the binding of AgNP surface and Ag ions at the chitin interface on the cuticular layer. Quantum chemistry calculations suggest that the toxicity is influenced by the ion state of silver (Ag^0, Ag^+, Ag^{2+}, and Ag^{3+} ions), with Ag^{3+} ions causing significant structural deformation of chitin. The binding mechanism of Ag ions to chitin occurs due to multiple types of chemical interactions. For instance, the interactions between Ag ions and chitin are primarily characterized as physisorption mechanisms. This interaction type refers to relatively weak, non-covalent interactions between the Ag ions and specific sites within the chitin molecule. This is indicated by the low interaction energy values observed in our study, typically <1 eV, affirming the non-covalent nature of the interactions. Also, the electrostatic component, was evidenced by SAPT0 analysis, plays a significant role in stabilizing the complexes. It highlights the attraction between charged species (Ag ions) and specific sites (such as -O12 and -O14) in the chitin molecule. These interactions are responsible for the binding of Ag ions to various functional groups within the chitin molecule, such as C–*O*–C from hexose, -NHCOCH3 from the N-acetyl group, and −CH2OH from the hydroxymethyl group. The specific nature of the interaction domain is influenced by the redox state of the Ag ions, suggesting a dependence on the Ag ion's oxidation state. Furthermore, the molecular docking simulations depicted the potential interaction of chitin with AgNP surfaces, elucidating the feasibility of interactions between the chitin monomer and the Ag ions present on the AgNP surfaces. The structural changes in chitin facilitate the diffusion of AgNPs through the cuticle and their subsequent accumulation within *A. salina* cells. This accumulation leads to cellular damage, as evidenced by confocal laser scanning microscopy. Overall, this study provides a comprehensive understanding of the toxicity mechanisms of AgNPs in *A. salina*, using it as a model organism, and these novel findings have potential implications for other chitin-based animals.

Declaration of competing interest

The authors declare that they have no known competing financial interests or personal relationships that could have appeared to influence the work reported in this paper.

Data availability

I have shared my data in repository

Aknowledgments

We are grateful to prof. Misbah for providing useful technical support in DFT calculation analysis. We are grateful to central analytical for supporting the microscopy analysis. ThaizRangel Miguel acknowledge funding from CNPq (Grant 350023/2020-4) and Central Analítica-UFC/CT-INFRA-FINEP/Pro-Equipamentos-CAPES/CNPq-SisNano-MCTI 2019 (Grant 442577/2019-2). SergimarPinheiro acknowledge funding from CAPES. Renato Grillo would also like to thank São Paulo Research Foundation, FAPESP (grant no. 2022/03219-2) and CNPq (grant no. 310846/2022-6). Antonio G. S. Filho acknowledge the financial support provided by CNPq (grants numbers: 305355/2020-8 and 442577/2019-2; grant number: 427498/2018-0).

References

Adams, C.P., Walker, K.A., Obare, S.O., Docherty, K.M., 2014. Size-dependent antimicrobial effects of novel palladium nanoparticles. PLoS One 9. https://doi.org/10.1371/journal.pone.0085981.

Ahamed, M., Akhtar, M.J., Alhadlaq, H.A., 2023. Synergistic toxicity of NiO nanoparticles and benzo[a]pyrene co-exposure in liver cells: role of free oxygen radicals induced oxidative stress. J. King Saud Univ. Sci. 35 https://doi.org/10.1016/j.jksus.2023.102750.

Alexiou, C., 2022. Emerging applications of magnetic nanoparticles in medicine – a personal perspective. Biochem. Biophys. Res. Commun. 633, 52–54. https://doi.org/10.1016/j.bbrc.2022.09.020.

An, H.J., Sarkheil, M., Park, H.S., Yu, I.J., Johari, S.A., 2019. Comparative toxicity of silver nanoparticles (AgNPs) and silver nanowires (AgNWs) on saltwater microcrustacean, Artemia salina. Comp. Biochem. Physiol., Part C: Toxicol. Pharmacol. 218, 62–69. https://doi.org/10.1016/j.cbpc.2019.01.002.

Anderson, D.T., 1967. Larval development and segment formation in the branchipod crustaceans Limnadia stanleyana King (Conchostraca) and Artemia salina (L.) (Anostraca). Aust. J. Zool. 15, 47–91.

Arulvasu, C., Jennifer, S.M., Prabhu, D., Chandhirasekar, D., 2014. Toxicity effect of silver nanoparticles in brine shrimp artemia. Sci. World J. https://doi.org/10.1155/2014/256919, 2014.

Asif, M., Sajid, H., Kosar, N., Mahmood, T., 2021. Effect of fluorination on the adsorption properties of aromatic heterocycles toward methyl halides : a quantum chemical study. Comput. Theor. Chem. 1204, 113394 https://doi.org/10.1016/j.comptc.2021.113394.

Ates, M., Danabas, D., Ertit Tastan, B., Unal, I., Cicek Cimen, I.C., Aksu, O., Kutlu, B., Arslan, Z., 2020. Assessment of oxidative stress on Artemia salina and Daphnia magna after exposure to Zn and ZnO nanoparticles. Bull. Environ. Contam. Toxicol. 104, 206–214. https://doi.org/10.1007/s00128-019-02751-6.

Ates, M., Daniels, J., Arslan, Z., Farah, I.O., Rivera, H.F., 2013. Comparative evolution of impact of Zn and ZnO nanoparticles on brine shrimp (Artemia salina) larvae: effects of particles size and solubility on toxicity. Environ. Sci. Process. Impacts 15, 225–233. https://doi.org/10.1016/j.dcn.2011.01.002.

Auffan, M., Bottero, J.Y., Chaneac, C., Rose, J., 2010. Inorganic manufactured nanoparticles: how their physicochemical properties influence their biological effects in aqueous environments. Nanomedicine 5, 999–1007. https://doi.org/10.2217/nnm.10.61.

Bachenheimer, L., Scherzer, R., Elliott, P., Stagon, S., Gasparov, L., Huang, H., 2017. Degradation mechanism of Ag nanorods for surface enhanced Raman spectroscopy. Sci. Rep. 7, 4–7. https://doi.org/10.1038/s41598-017-16580-2.

Bai, W., Zhang, Z., Tian, W., He, X., Ma, Y., Zhao, Y., Chai, Z., 2010. Toxicity of zinc oxide nanoparticles to zebrafish embryo: a physicochemical study of toxicity mechanism. J. Nanoparticle Res. 12, 1645–1654. https://doi.org/10.1007/s11051-009-9740-9.

Boyle, N.M.O., Tenderholt, A.L., Langner, K.M., 2007. Software news and updates cclib : a library for package-independent computational chemistry algorithms. J. Comput. Chem. 29, 839–845. https://doi.org/10.1002/jcc.

Cedervall, T., Lynch, I., Lindman, S., Berggard, T., Thulin, E., Nilsson, H., Dawson, K.A., Linse, S., 2007. Understanding the nanoparticle-protein corona using methods to quantify exchange rates and affinities of proteins for nanoparticles. Proc. Natl. Acad. Sci. USA 104, 2050–2055. https://doi.org/10.1073/pnas.0608582104.

Chang, S., 1995. Physiological and biochemical changes during the molt cycle in decapod crustaceans : an overview. J. Exp. Mar. Biol. Ecol. 193, 1–14.

Chatzigoulas, A., Karathanou, K., Dellis, D., Cournia, Z., 2018. NanoCrystal: a web-based crystallographic tool for the construction of nanoparticles based on their crystal habit. J. Chem. Inf. Model. 58 https://doi.org/10.1021/acs.jcim.8b00269.

Christian, P., Von Der Kammer, F., Baalousha, M., Hofmann, T., 2008. Nanoparticles: structure, properties, preparation and behaviour in environmental media. Ecotoxicology 17, 326–343. https://doi.org/10.1007/s10646-008-0213-1.

Cruzeiro, C., Rocha, E., João, M., 2017. Determination of 54 pesticides in waters of the Iberian Douro River estuary and risk assessment of environmentally relevant mixtures using theoretical approaches and Artemia salina and Daphnia magna bioassays. Ecotoxicol. Environ. Saf. 145, 126–134. https://doi.org/10.1016/j.ecoenv.2017.07.010.

Damas-Souza, D.M., Nunes, R., Carvalho, H.F., 2019. An improved acridine orange staining of DNA/RNA. Acta Histochem. 121, 450–454. https://doi.org/10.1016/j.acthis.2019.03.010.

De Paiva Pinheiro, S.K., De Medeiros Chaves, M., Rangel Miguel, T.B.A., De Freitas Barros, F.C., Farias, C.P., Ferreira, O.P., De Castro Miguel, E., 2020. Toxic effects of silver nanoparticles on the germination and root development of lettuce (Lactuca sativa). Aust. J. Bot. 68, 127–136. https://doi.org/10.1071/BT19170.

de Paiva Pinheiro, S.K., Lima, A.K.M., Miguel, T.B.A.R., Pireda, S., Fechine, P.B.A., Souza Filho, A.G., de Castro Miguel, E., 2023. Acute toxicity of titanium dioxide microparticles in Artemia sp. nauplii instar I and II. Microsc. Res. Tech. 86, 636–647. https://doi.org/10.1002/jemt.24312.

Durán, N., Rolim, W.R., Durán, M., Fávaro, W.J., Seabra, A.B., 2019. NANOTOXICOLOGIA de NANOPARTÍCULAS de PRATA: TOXICIDADE EM ANIMAIS E HUMANOS. Quim. Nova 42, 206–213.

Eckhardt, S., Brunetto, P.S., Gagnon, J., Priebe, M., Giese, B., Fromm, K.M., 2013. Nanobio silver: its interactions with peptides and bacteria, and its uses in medicine. Chem. Rev. 113, 4708–4754. https://doi.org/10.1021/cr300288v.

Edison, T.J.I., Sethuraman, M.G., 2012. Instant green synthesis of silver nanoparticles using Terminalia chebula fruit extract and evaluation of their catalytic activity on reduction of methylene blue. Process Biochem 47, 1351–1357. https://doi.org/10.1016/j.procbio.2012.04.025.

Forini, M.M.L., Pontes, M.S., Antunes, D.R., Lima, P.H.C. De, Santos, J.S., Santiago, E.F., Grillo, R., 2022. Nano-enabled weed management in agriculture_ from strategic design to enhanced herbicidal activity. Plant Nano Biol 1, 100008. https://doi.org/10.1016/j.plana.2022.100008.

Freeman, J.A., 1986. Epidermal cell proliferation during thoracic development in larvae of Artemia. J. Crustac Biol. 6, 37–48. https://doi.org/10.1163/193724086X00703.

Garaventa, F., Gambardella, C., Di Fino, A., Pittore, M., Faimali, M., 2010. Swimming speed alteration of Artemia sp. and Brachionus plicatilis as a sub-lethal behavioural end-point for ecotoxicological surveys. Ecotoxicology 19, 512–519. https://doi.org/10.1007/s10646-010-0461-8.

Geisler-Lee, J., Wang, Q., Yao, Y., Zhang, W., Geisler, M., Li, K., Huang, Y., Chen, Y., Kolmakov, A., Ma, X., 2013. Phytotoxicity, accumulation and transport of silver nanoparticles by Arabidopsis thaliana. Nanotoxicology 7, 323–337. https://doi.org/10.3109/17435390.2012.658094.

Ghadirian, S., Karbasi, S., Kharazi, A.Z., Setayeshmehr, M., 2023. Evaluation of the effects of halloysite nanotubes on physical, mechanical, and biological properties of polyhydroxy butyrate electrospun scaffold for cartilage tissue engineering applications. J. Polym. Environ. 249 https://doi.org/10.1007/s10924-023-03024-4.

Ghouri, F., Shahid, M.J., Liu, J., Lai, M., Sun, L., Wu, J., Liu, X., Ali, S., Shahid, M.Q., 2023. Polyploidy and zinc oxide nanoparticles alleviated Cd toxicity in rice by modulating oxidative stress and expression levels of sucrose and metal-transporter genes. J. Hazard Mater. 448 https://doi.org/10.1016/j.jhazmat.2023.130991.

Jafari, A., Rashidipour, M., Kamarehi, B., Alipour, S., Ghaderpoori, M., 2022. Toxicity of green synthesized TiO2 nanoparticles (TiO2 NPs) on zebra fish. Environ. Res. 212 https://doi.org/10.1016/j.envres.2022.113542.

Jin, X., Li, M., Wang, J., Marambio-Jones, C., Peng, F., Huang, X., Damoiseaux, R., Hoek, E.M.V., 2010. High-throughput screening of silver nanoparticle stability and bacterial inactivation in aquatic media: influence of specific ions. Environ. Sci. Technol. 44, 7321–7328. https://doi.org/10.1021/es100854g.

Johari, S.A., Rasmussen, K., Gulumian, M., Ghazi-Khansari, M., Tetarazako, N., Kashiwada, S., Asghari, S., Park, J.W., Yu, I.J., 2019. Introducing a new standardized nanomaterial environmental toxicity screening testing procedure, ISO/TS 20787: aquatic toxicity assessment of manufactured nanomaterials in saltwater Lakes using Artemia sp. nauplii. Toxicol. Mech. Methods 29, 95–109. https://doi.org/10.1080/15376516.2018.1512695.

Khairul Azri, A.A., Mohd Jasni, M.S., Wan Muhamad Hatta, S.F., Islam, M.A., Abdul Wahab, Y., Mekhilef, S., Ker, P.J., 2023. Advancement in thermophotovoltaic technology and nanoparticle incorporation for power generation. Sol. Energy 259, 279–297. https://doi.org/10.1016/j.solener.2023.05.018.

Khan, S., Yar, M., Kosar, N., Ayub, K., Arshad, M., Zahid, M.N., Mahmood, T., 2020. First-principles study for exploring the adsorption behavior of G-series nerve agents on graphdyine surface. Comput. Theor. Chem. 1191, 113043 https://doi.org/10.1016/j.comptc.2020.113043.

Kosa, S.A., Zaheer, Z., 2022. Biogenic fabrication of silver nanoparticles, oxidative dissolution and antimicrobial activities. J. Saudi Chem. Soc. 26 https://doi.org/10.1016/j.jscs.2021.101414.

Krishnan, V., Prakash, J.S., Manigandan, V., Venkatasubbu, G.D., Pugazhendhi, A., Brindhadevi, K., Kalaivani, T., 2022. Synthesis of mesoporous SiO2 nanoparticles and toxicity assessment in early life stages of zebrafish. Microporous Mesoporous Mater. 330 https://doi.org/10.1016/j.micromeso.2021.111573.

Lacave, J.M., Fanjul, Á., Bilbao, E., Gutierrez, N., Barrio, I., Arostegui, I., Cajaraville, M. P., Orbea, A., 2017. Acute toxicity, bioaccumulation and effects of dietary transfer of silver from brine shrimp exposed to PVP/PEI-coated silver nanoparticles to zebrafish. Comp. Biochem. Physiol., Part C: Toxicol. Pharmacol. 199, 69–80. https://doi.org/10.1016/j.cbpc.2017.03.008.

Lavens, P., Sorgeloos, P., 1996. Manual on the production and use of live food for aquaculture. Fish. Tech. Pap. 361.

Lee, W.M., An, Y.J., Yoon, H., Kweon, H.S., 2008. Toxicity and bioavailability of copper nanoparticles to the terrestrial plants mung bean (Phaseolus radiatus) and wheat (Triticum aestivum): plant agar test for water-insoluble nanoparticles. Environ. Toxicol. Chem. 27, 1915–1921. https://doi.org/10.1897/07-481.1.

Legge, F.S., Nyberg, G.L., Peel, J.B., 2001. DFT calculations for Cu- , Ag- , and Au-containing molecules. J. Phys. Chem. A 105, 7905–7916.

Machanlou, M., Ziaei-nejad, S., Johari, S.A., Banaei, M., 2023. Study on the hematological toxicity of Cyprinus carpio exposed to water-soluble fraction of crude oil and TiO2 nanoparticles in the dark and ultraviolet. Chemosphere 343. https://doi.org/10.1016/j.chemosphere.2023.140272.

Maia, M.T., Delite, F.S., da Silva, G.H., Ellis, L.J.A., Papadiamantis, A.G., Paula, A.J., Lynch, I., Martinez, D.S.T., 2023. Combined toxicity of fluorescent silica nanoparticles with cadmium in Ceriodaphnia dubia: interactive effects of natural organic matter and green algae feeding. J. Hazard Mater. 461 https://doi.org/10.1016/j.jhazmat.2023.132623.

Manfra, L., Tornambè, A., Savorelli, F., Rotini, A., Canepa, S., Mannozzi, M., Cicero, A. M., 2014. Ecotoxicity of diethylene glycol and risk assessment for marine environment. J. Hazard Mater. 284, 130–135. https://doi.org/10.1016/j.jhazmat.2014.11.008.

Margiotta, E., Fonseca Guerra, C., 2021. SARS-CoV spike proteins can compete for electrolytes in physiological fluids according to structure-based quantum-chemical calculations. Comput. Theor. Chem. 1204 https://doi.org/10.1016/j.comptc.2021.113392.

Mascarenhas-Melo, F., Mathur, A., Murugappan, S., Sharma, A., Tanwar, K., Dua, K., Singh, S.K., Mazzola, P.G., Yadav, D.N., Rengan, A.K., Veiga, F., Paiva-Santos, A.C., 2023. Inorganic nanoparticles in dermopharmaceutical and cosmetic products: properties, formulation development, toxicity, and regulatory issues. Eur. J. Pharm. Biopharm. 192, 25–40. https://doi.org/10.1016/j.ejpb.2023.09.011.

Mcgillicuddy, E., Murray, I., Kavanagh, S., Morrison, L., Fogarty, A., Cormican, M., Dockery, P., Prendergast, M., Rowan, N., Morris, D., 2017. Silver nanoparticles in the environment : sources , detection and ecotoxicology. Sci. Total Environ. 575, 231–246. https://doi.org/10.1016/j.scitotenv.2016.10.041.

Mehennaoui, K., Cambier, S., Minguez, L., Serchi, T., Guérold, F., Gutleb, A.C., Giamberini, L., 2021. Sub-chronic effects of AgNPs and AuNPs on Gammarus fossarum (Crustacea Amphipoda): from molecular to behavioural responses. Ecotoxicol. Environ. Saf. 210 https://doi.org/10.1016/j.ecoenv.2020.111775.

Meng, X.Y., Zhang, H.X., Mezei, M., Cul, M., 2012. Molecular Docking: a powerful approach for structure-based drug discovery. Curr. Comput. Aided Drug Des. 7, 146–157.

Meyer, D.E., Curran, M.A., Gonzalez, M. a, Agency, U.S.E.P., King, W.M.L., 2009. An examination of existing data for the industrial manufacture and use of nanocomponents and their role in the life cycle impact of nanoproducts national risk management research laboratory ph : 513-569-7194 supporting information the following 10 pages c. Environ. Sci. Technol. 43, 1256–1263.

Mezacasa, A.V., Queiroz, A.M., Graciano, D.E., Pontes, M.S., Santiago, E.F., Oliveira, I.P., Lopez, A.J., Casagrande, G.A., Scherer, M.D., Reis, D.D., Oliveira, S.L., Caires, A.R.L., 2020. Journal of Photochemistry & Photobiology A : chemistry E ff ects of gold nanoparticles on photophysical behaviour of chlorophyll and pheophytin. J. Photochem. Photobiol. Chem. 389, 112252 https://doi.org/10.1016/j.jphotochem.2019.112252.

Monteiro, M., Medina, L., Casanova, P., Espinola, M., Machado, A., Ribeiro, A.A., Riquet, A., Azevedo Rangel Miguel, T.B., de Castro Miguel, E., Quevedo Nogueira, R. E.F., 2023. Evaluation of the acute toxicity by Artemia salina of hydroxyapatite nanoparticles obtained via sol-gel in an aqueous medium without using additives. Ceram. Int. 49, 38509–38518. https://doi.org/10.1016/j.ceramint.2023.09.181.

Morgana, S., Estévez-Calvar, N., Gambardella, C., Faimali, M., Garaventa, F., 2018. A short-term swimming speed alteration test with nauplii of Artemia franciscana. Ecotoxicol. Environ. Saf. 147, 558–564. https://doi.org/10.1016/j.ecoenv.2017.09.026.

Muthukrishnan, S., Kumar, T.S., Rao, M.V., 2017. Anticancer activity of biogenic nanosilver and its toxicity assessment on Artemia salina - evaluation of mortality , accumulation and elimination : an experimental report. J. Environ. Chem. Eng. 5, 1685–1695. https://doi.org/10.1016/j.jece.2017.03.004.

Narayan, R., Gadag, S., Garg, S., Nayak, U.Y., 2022. Understanding the E Ff Ect of Functionalization on Loading Capacity and Release of Drug from Mesoporous Silica Nanoparticles : A Computationally Driven Study. https://doi.org/10.1021/acsomega.1c03618.

Nunes, B.S., Carvalho, F.D., Guilhermino, L.M., Van Stappen, G., 2006. Use of the genus Artemia in ecotoxicity testing. Environ. Pollut. 144, 453–462. https://doi.org/10.1016/j.envpol.2005.12.037.

Ocaranza-Joya, V.S., Manjarrez-Alcivar, I., Ruizgonzález, L.E., Guerrero-Galván, S.R., Vega-Villasante, F., 2019. Sensitivity of different stages of Artemia franciscana to potassium dichromate. Pan Am. J. Aquat. Sci. 14, 8–12.

OECD, 2004. OECD guideline for testing of chemical, guideline for testing of chemicals. Section 2. https://doi.org/10.1787/9789264069947-en.

Papolu, P., Bhogi, A., 2023. Green synthesis of various metal oxide nanoparticles for the environmental remediation-An overview. Mater. Today Proc. https://doi.org/10.1016/j.matpr.2023.04.544.

Piccapietra, F., Allue, C.G., Sigg, L., Behra, R., 2012. Intracellular silver accumulation in Chlamydomonas reinhardtii upon exposure to carbonate coated silver nanoparticles and silver nitrate. Environ. Sci. Technol. 46, 7390–7397. https://doi.org/10.1021/es300734m.

Pontes, M.S., Antunes, D.R., Oliveira, I.P., Forini, M.M.L., Santos, J.S., Arruda, G.J., Caires, A.R.L., Santiago, E.F., Grillo, R., 2021. Chitosan/tripolyphosphate nanoformulation carrying paraquat: insights on its enhanced herbicidal activity. Environ. Sci.: Nano 8, 1336–1351. https://doi.org/10.1039/D0EN01128B.

Pontes, M.S., Santos, J.S., Fernandes, S.Y., Oliveira, I.P., Miguel, T.B.A.R., Miguel, E.C., Arruda, G.J., Grillo, R., Caires, A.R.L., Santiago, E.F., 2023. In: Al-Khayri, J.M., Alnaddaf, L.M., Jain, S.M. (Eds.), Interactions of Nanomaterials with Plant Pigments BT - Nanomaterial Interactions with Plant Cellular Mechanisms and Macromolecules and Agricultural Implications. Springer International Publishing, Cham, pp. 93–131. https://doi.org/10.1007/978-3-031-20878-2_5.

Rekulapally, R., Chavali, L.N.M., Idris, M.M., Singh, S., 2019. 2019. Toxicity of TiO 2 , SiO 2 , ZnO, CuO, Au and Ag engineered nanoparticles on hatching and early nauplii of Artemia sp. PeerJ. https://doi.org/10.7717/peerj.6138.

Rhazouani, A., Gamrani, H., Ed-Day, S., Lafhal, K., Boulbaroud, S., Gebrati, L., Fdil, N., Aziz, F., 2023. Sub-acute toxicity of graphene oxide (GO) nanoparticles in male mice after intraperitoneal injection: behavioral study and histopathological evaluation. Food Chem. Toxicol. 171, 2–11. https://doi.org/10.1016/j.fct.2022.113553.

Sajid, H., Mahmood, T., Ayub, K., 2018. High sensitivity of polypyrrole sensor for uric acid over urea , acetamide and sulfonamide : a density functional theory study. Synth. Met. 235, 49–60. https://doi.org/10.1016/j.synthmet.2017.11.008.

Santiago, E.F., Pontes, M.S., Arruda, G.J., Caires, A.R.L., Colbeck, I., Maldonado-Rodriguez, R., Grillo, R., 2020. In: Fraceto, L.F., de Castro, S.S., L, V., Grillo, R., Ávila, D., Caixeta Oliveira, H., Lima, R. (Eds.), Understanding the Interaction of Nanopesticides with Plants BT - Nanopesticides: from Research and Development to Mechanisms of Action and Sustainable Use in Agriculture. Springer International Publishing, Cham, pp. 69–109. https://doi.org/10.1007/978-3-030-44873-8_4.

Santos-Rasera, J.R., Monteiro, R.T.R., de Carvalho, H.W.P., 2022. Investigation of acute toxicity, accumulation, and depuration of ZnO nanoparticles in Daphnia magna. Sci. Total Environ. 821 https://doi.org/10.1016/j.scitotenv.2022.153307.

Sarfaraz, S., Yar, M., Ans, M., Gilani, A., Ludwig, R., Hashmi, D.M.A., Hussain, M., 2022. RSC advances. RSC Adv. 12, 3909–3923. https://doi.org/10.1039/d1ra08738j.

Sarkheil, M., Johari, S.A., An, H.J., Asghari, S., Park, H.S., Sohn, E.K., Yu, I.J., 2018. Acute toxicity, uptake, and elimination of zinc oxide nanoparticles (ZnO NPs) using saltwater microcrustacean, Artemia franciscana. Environ. Toxicol. Pharmacol. 57, 181–188. https://doi.org/10.1016/j.etap.2017.12.018.

Sendra, M., Blasco, J., Araújo, C.V.M., 2018. Is the cell wall of marine phytoplankton a protective barrier or a nanoparticle interaction site? Toxicological responses of Chlorella autotrophica and Dunaliella salina to Ag and CeO2 nanoparticles. Ecol. Indicat. 95, 1053–1067. https://doi.org/10.1016/j.ecolind.2017.08.050.

Sorgeloos, P., Remiche-Van Der Wielen, C., Persoone, G., 1978. The use of Artemia nauplii for toxicity tests-A critical analysis. Ecotoxicol. Environ. Saf. 2, 249–255. https://doi.org/10.1016/S0147-6513(78)80003-7.

Tosco, T., Sethi, R., 2018. Human health risk assessment for nanoparticle-contaminated aquifer systems. Environ. Pollut. 239, 242–252. https://doi.org/10.1016/j.envpol.2018.03.041.

Turi, L., Dannenberg, J.J., 1993. Correcting for basis set superposition error in aggregates containing more than two molecules : ambiguities in the calculation of the counterpoise correction. J. Phys. Chem. 97, 2488–2490.

Turney, J.M., Simmonett, A.C., Parrish, R.M., Hohenstein, E.G., Evangelista, F.A., Justin, T., Mintz, B.J., Burns, L.A., Wilke, J.J., Abrams, M.L., Russ, N.J., Leininger, M.L., Janssen, C.L., Seidl, E.T., Allen, W.D., Schaefer, H.F., King, R.A., Valeev, E.F., Sherrill, C.D., Crawford, T.D., Wiley, J., 2012. PSI 4 : an open-source ab initio electronic structure program. WIREs Comput Mol Sci 2, 556–565. https://doi.org/10.1002/wcms.93.

Tyagi, P.K., Rizvi, T., Kapse, A.V., 2023. Evaluate the toxicity of silver nanoparticles by chemical and green synthesis methods. Mater. Today Proc. 78, 80–85. https://doi.org/10.1016/j.matpr.2022.11.200.

Wang, P., Zhang, B., Zhang, H., He, Y., Ong, C.N., Yang, J., 2019. Metabolites change of Scenedesmus obliquus exerted by AgNPs. J. Environ. Sci. (China) 76, 310–318. https://doi.org/10.1016/j.jes.2018.05.017.

Warner, A.H., Matheson, C., 1998. Release of proteases from larvae of the brine shrimp Artemia franciscana and their potential role during the molting process. Comp. Biochem. Physiol. 119, 255–263.

Weisz, P.B., 1946. Marine Biological Laboratory, vol. 91. The University of Chicago Press, pp. 119–140.

Xiu, Z.M., Zhang, Q.B., Puppala, H.L., Colvin, V.L., Alvarez, P.J.J., 2012. Negligible particle-specific antibacterial activity of silver nanoparticles. Nano Lett. 12, 4271–4275. https://doi.org/10.1021/nl301934w.

Yadav, P., Bandyopadhyay, A., Chakraborty, A., Sarkar, K., 2018. Enhancement of anticancer activity and drug delivery of chitosan-curcumin nanoparticle via molecular docking and simulation analysis. Carbohydr. Polym. 182, 188–198. https://doi.org/10.1016/j.carbpol.2017.10.102.

Yan, Y., Wen, Z., Wang, X., Huang, S., 2016. Addressing recent docking challenges: a hybrid strategy to integrate template-based and free protein-protein docking. Proteins: Struct., Funct., Bioinf. 85, 497–512. https://doi.org/10.1002/prot.25234.

Yang, R., Gu, Y., Qin, J., Liu, Qingqing, Liu, Qing, 2023. Potential role of Chinese medicine nanoparticles to treat coronary artery disease. Heliyon 9. https://doi.org/10.1016/j.heliyon.2023.e19766, 1-11.

Yu, s. j, Yin, Y., Liu, j. f, 2013. Silver nanoparticles in the environment. Environ. Sci. Process. Impacts 15, 78–92. https://doi.org/10.1039/c2em30595j.

Zeng, L., Peng, Q., Li, Q., Bi, Y., Kong, F., Wang, Z., Tan, S., 2023. Synthesis, characterization, biological activity, and in vitro digestion of selenium nanoparticles stabilized by Antarctic ice microalgae polypeptide. Bioorg. Chem. 141 https://doi.org/10.1016/j.bioorg.2023.106884.

Zhang, J., Xie, X., Li, Q., Wang, J., Zhang, S., 2023. Combined toxic effects of TiO2 nanoparticles and organochlorines on Chlorella pyrenoidosa in karst area natural waters. Aquat. Toxicol. 257 https://doi.org/10.1016/j.aquatox.2023.106442.

Zhang, X., Yuan, J., Li, F., Xiang, J., 2021. Chitin synthesis and degradation in Crustaceans : a genomic view and application. Mar. Drugs 153, 1–23.